

Chapter 1

Modelling chemotaxis of microswimmers: from individual to collective behavior

B. Liebchen and H. Löwen

*Institut für Theoretische Physik II: Weiche Materie
Heinrich-Heine-Universität Düsseldorf
Universitätsstr. 1
D - 40225 Düsseldorf*

We discuss recent progress in the theoretical description of chemotaxis by coupling the diffusion equation of a chemical species to equations describing the motion of sensing microorganisms. In particular, we discuss models for autochemotaxis of a single microorganism which senses its own secretion leading to phenomena such as self-localization and self-avoidance. For two heterogeneous particles, chemotactic coupling can lead to predator-prey behavior including chase and escape phenomena, and to the formation of active molecules, where motility spontaneously emerges when the particles approach each other. We close this review with some remarks on the collective behavior of many particles where chemotactic coupling induces patterns involving clusters, spirals or traveling waves.

1. Introduction

Chemotaxis plays a crucial role in the life of many microorganisms. It allows them to navigate towards food sources and away from toxins, but is also used for signaling underlying self-organization in multicellular communities. Here, microorganisms sense the concentration of a chemical and adjust their motion to the chemical gradient:¹⁻³ if the corresponding chemical signal is externally imposed and, say, a food source, microorganisms will try to move up the gradient towards the food source (“chemoattraction”, or “positive chemotaxis”). In the opposite case of a toxin, microorganisms migrate down the gradient (“chemorepulsion”, or “negative chemotaxis”).⁴

Many microorganisms can produce the chemicals to which they respond themselves and use chemotaxis for signaling. Here, chemotactic behaviour

strongly couples to *chemical kinetics*, which is the main topic of the present book.

In this book-chapter we review recent progress in the theoretical description of chemotaxis beyond present textbook knowledge. Modelling of chemotaxis concerns the coupling between the dynamics of the chemical, as described by the diffusion equation together with appropriate source and sink terms, and the motion of microorganisms. Therefore we discuss the basic equations for the chemical diffusion and the motion of bacteria (or other microorganisms) which is coupled to the chemical field. We then proceed step-by-step from few to many bacteria, where the chemotactic response of a bacterium to chemicals produced by another one lead to chemical interactions, or signaling, among microorganisms.

The simplest case of a single bacterium (or "particle") which senses its own secretion is discussed first. This case, also called *autochemotaxis*, is both of biological relevance and of fundamental importance as it may lead to effects such as self-localization. This in turn leads to dynamical scaling laws for the mean-square-displacement of the particle which are different from ordinary diffusion and are therefore of general interest.⁵ We then proceed to a two particle predator and prey system governed by chemotactic sensing and finally discuss the general case of many (more than two) particles which probably plays a key role for dynamical cluster formation and other patterns. Since chemotaxis allows microorganisms to navigate, and also allows to steer synthetic microswimmers, it is linked to the the rapidly expanding research field of active particles, as for recent reviews see.⁶⁻⁹

2. Basics: diffusion of chemicals in different spatial dimensions and chemotactic coupling

2.1. Diffusing chemicals around static (non-moving) point sources

To set a theoretical framework for chemotaxis we first explore the kinetics of the chemical that constitutes the chemotactic signal. We start with the diffusion equation for a chemical concentration field $c(\vec{r}, t)$ in solution with a point source emitting the chemical with a rate $\lambda_e(t)$, which may generally depend on time, at fixed position \vec{r}_0 :

$$\frac{\partial c(\vec{r}, t)}{\partial t} = D_c \Delta c(\vec{r}, t) - \mu c(\vec{r}, t) + \lambda_e(t) \delta(\vec{r} - \vec{r}_0) \quad (1)$$

Here, D_c is the diffusion coefficient of the chemical in solution. The chemical may also evaporate (or disappear) with a rate μ , e.g. due to another chemical reaction. In the following, we focus on constant emission rates. The diffusion equation (1) can be considered in $d = 1, 2, 3$ spatial dimensions which $d = 1$ corresponding to an effective slab and $d = 2$ to an effective cylindrical geometry. Accordingly Δ denotes the Laplacian operator in d spatial dimensions. For an instantaneous onset of chemical emission at $t = 0$, i.e. $\lambda_e(t) = \lambda_e \Theta(t)$, where $\Theta(t)$ denotes the unit step function and $\mu = 0$, the solution of Eqn. (1) is given in d dimensions by¹⁰

$$c(\vec{r}, t) = \lambda_e \int_0^t dt' \frac{1}{(4\pi D_c |t - t'|)^{\frac{d}{2}}} \exp\left(-\frac{(\vec{r} - \vec{r}_0)^2}{4D_c |t - t'|}\right) \quad (2)$$

By substituting $t' \rightarrow s := (\vec{r} - \vec{r}_0)^2 / (4D_c |t - t'|)$, this expression can be also written in terms of the upper incomplete Gamma function $\Gamma(a, b) = \int_b^\infty e^{-x} x^{a-1} dx$

$$c(\vec{r}, t) = \frac{\lambda |\vec{r} - \vec{r}_0|^{2-d}}{4\pi^{d/2} D_c} \Gamma\left(\frac{d}{2} - 2, \frac{(\vec{r} - \vec{r}_0)^2}{4D_c t}\right) \quad (3)$$

Expression (2) can be generalized, for $\mu \neq 0$ to

$$c(\vec{r}, t) = \lambda_e \int_0^t dt' \frac{1}{(4\pi D_c |t - t'|)^{\frac{d}{2}}} \exp\left(-\frac{(\vec{r} - \vec{r}_0)^2}{4D_c |t - t'|} - \mu |t - t'|\right) \quad (4)$$

In many cases, the dynamics of the chemical is fast compared to all other relevant timescales in a given system (e.g. the response time of a microorganism). In these cases, we are mainly interested in the chemical steady state profile, corresponding to $\dot{c} = 0$ in Eq. (1). This steady state problem is formally equivalent to screened electrostatics, or in other words, to linear Debye-Hückel theory of screening¹¹ with an inverse screening length κ now given by

$$\kappa = \sqrt{\mu/D_c} \quad (5)$$

while without evaporation ($\mu = 0$) we have an analogy to the Poisson equation of ordinary (unscreened) electrostatics. Therefore, in various spatial dimensions d the solutions, for a localized initial state, are as follows:

- (i) In $d = 1$, there is an "exponential orbital" around the secreting source fixed at the origin of the coordinate system such that for a spatial coordinate x the concentration field is for $\mu > 0$

$$c(x) = \frac{\lambda_e}{\sqrt{4D_c\mu}} \exp(-\kappa|x|) \quad (6)$$

For $\mu = 0$, the steady state solution becomes unphysical; in that case, the time-dependent solution does not converge to a steady state but increases forever.

- (ii) For $d = 2$, there is a "Macdonald orbital"

$$c(r) = \frac{\lambda_e}{D_c} K_0(\kappa r) \quad (7)$$

with r denoting the radial distance in two dimensions from the source. Here $K_0(x)$ is a Macdonald function (or modified Bessel function) (see e.g. Eqn (39) in¹²). Like in $d = 1$, for $\mu = 0$ the chemical density does not converge and the steady state solution becomes unphysical.

- (iii) Finally, for $d = 3$, there is a radial-symmetric Debye-Hückel (or Yukawa) orbital around the point source

$$c(r) = \frac{\lambda_e}{4\pi D_c r} \exp(-\kappa r) \quad (8)$$

which reduces for $\mu = 0$ to the classical Coulomb solution

$$c(r) = \frac{\lambda_e}{4\pi D_c r} \quad (9)$$

again with r denoting the radial distance from the point source.

2.2. Moving point sources

When the point source is moving with a constant velocity \vec{v} , the general diffusion equation for constant emission rate is

$$\frac{\partial c(\vec{r}, t)}{\partial t} = D_c \Delta c(\vec{r}, t) - \mu c(\vec{r}, t) + \lambda_e \delta(\vec{r} - \vec{r}_0 - \vec{v}t) \quad (10)$$

By a Galilean transformation from the laboratory frame into the moving particle frame this equation can be transformed such that it reads under steady state conditions as follows

$$-D_c \Delta c(\vec{r}) + (\vec{v} \cdot \vec{\nabla}) c(\vec{r}) + \mu c(\vec{r}) = \lambda_e \delta(\vec{r}) \quad (11)$$

Solutions of Eq. (11) go beyond textbook knowledge and have not been discussed yet in this context. In general, the Green's function associated with Eq. (11) can be expressed as a Fourier integral as

$$c(\vec{r}) = \frac{\lambda}{(2\pi)^d} \int_{-\infty}^{\infty} d^d k \frac{e^{-i\vec{k} \cdot \vec{r}}}{D_c \vec{k}^2 + i\vec{v} \cdot \vec{k} + \mu} \quad (12)$$

Evaluating this integral in one spatial dimension ($d = 1$) yields a solution consisting of two exponentials with different decay lengths in the front and in the rear of the moving source:

$$c(x) = \frac{\lambda_e}{\sqrt{4D_c\mu}} \begin{cases} e^{-\chi_+ |x|} & \text{for } x \geq 0 \\ e^{-\chi_- |x|} & \text{for } x < 0 \end{cases} \quad (13)$$

$$\text{with } \chi_{\pm} = \sqrt{\frac{\mu}{D_c} + \frac{v^2}{4D_c^2}} \pm \frac{v}{2D_c} \quad (14)$$

This solution is plotted in (1). Clearly, increasing the speed of the source enhances the front-rear asymmetry while at $v = 0$ we recover the solution (6) of a static point source. Increasing the evaporation rate basically decreases the range of the chemical concentration around the source.

For the corresponding solution in two dimensions, we find:

$$c(\vec{r}) = \frac{\lambda_e}{D_c} K_0(\tilde{\kappa}r) \exp\left(-\frac{\vec{v} \cdot \vec{r}}{2D_c}\right); \quad \text{with } \tilde{\kappa} = \sqrt{\frac{\mu}{D_c} + \frac{\vec{v}^2}{4D_c^2}} \quad (15)$$

and in three dimensions:

$$c(\vec{r}) = \frac{\lambda_e}{4\pi D_c r} \exp\left(-\tilde{\kappa}r - \frac{\vec{v} \cdot \vec{r}}{2D_c}\right) \quad (16)$$

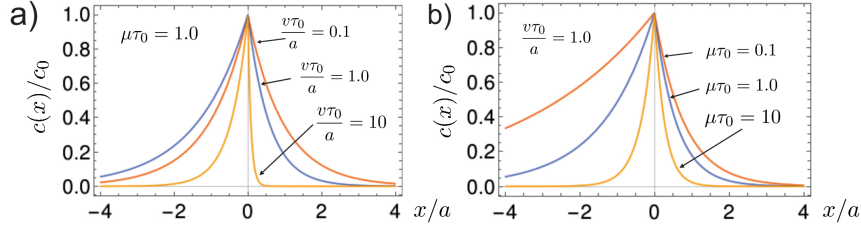


Fig. 1. Reduced concentration field $c(x)/c_0$ as a function of reduced distance x/a to the moving source. This is the steady state solution for the one-dimensional diffusion equation of a point source moving with a velocity v with constant emission rate λ_e for various relative speeds (a) and relative evaporation rates (b). All length and time scales are given in terms of $a = \sqrt{D_c/\lambda_e}$ and $\tau_0 = 1/\lambda_e$, and $c_0 = 1/(2a\sqrt{\mu\tau_0})$. The parameters are: (a) $v\tau_0/a = 0.1, 1.0, 10$ at $\mu\tau_0 = 1$ and (b) $\mu\tau_0 = 0.1, 1.0, 10$ at $v\tau_0/a = 1$.

For $\mu = 0$, in a coordinate system whose x -axis points along \vec{v} , the three dimensional solution reduces to

$$c(\vec{r}) = \frac{\lambda_e}{4\pi D_c r} \exp\left[-\frac{|\vec{v}|(x + |\vec{r}|)}{2D_c}\right] \quad (17)$$

Remarkably in the rear of the moving source ($x < 0$ at $y = z = 0$ such that $x + r = 0$) the chemical concentration decays algebraically as $1/|x|$ while in all other directions it decays with a Yukawa-behavior as $\exp(-vx/D_c)/x$, i.e. algebraically for $r \ll \sqrt{D_c/\mu}$ and exponentially at longer distances. This asymmetry indicates the significance of the source trail and a memory effect about the past of the secreting particle.

2.3. Chemotactic coupling and secreting particle dynamics

For chemotaxis in its simplest form, the particle directs its motion according to the gradient of the chemical field. We describe this coupling to the chemical concentration as an effective force

$$\vec{F} = \alpha \nabla c(\vec{r}, t) \quad (18)$$

acting on the particle. Here positive α values represent “positive” chemotaxis or “chemoattraction” whereas negative α values represent “negative” chemotaxis or “chemorepulsion”. The linear coupling to the gradient is the simplest possible form, but other couplings like logarithmic ones are also

conceivable and probably relevant for microbiological systems¹³ where

$$\vec{F} = \alpha \vec{\nabla} \ln c(\vec{r}, t) = \alpha \frac{\vec{\nabla} c(\vec{r}, t)}{c(\vec{r}, t)} \quad (19)$$

A more complicated coupling involves a concentration dependent prefactor α as proposed in Ref.¹⁴ We will basically use and discuss formula (18) in the sequel.

The effective chemotactic force typically acts on a completely overdamped particle with position $\vec{r}_p(t)$, leading to the following equation of motion:

$$\gamma \frac{d}{dt} \vec{r}_p(t) = \alpha \nabla c(\vec{r}_p(t), t) \quad (20)$$

Here, γ is the Stokes drag coefficient. If necessary, additional noise terms can be added to Eq. (20) in order to model the stochastic collisions of the particle with the solvent molecules. Here we neglect any hydrodynamic flow effects stemming from a finite radius of the point source are neglected. Their inclusion would require a more sophisticated analysis.

3. Autochemotaxis for a single particle

If a single particle emits a chemical to which it responds itself, we call this “autochemotaxis”. Here, Tsori and de Gennes¹⁵ have coupled the chemical diffusion equation to an equation of motion for a particle. For the chemoattractant case at vanishing evaporation rate $\mu = 0$, they have found “*self-trapping*” of the particle in a spatial dimension $d = 1, 2$ but not for $d = 3$. This implies that a particle traps itself if moves towards the chemical which it has secreted in the past. The concept of “perfect” self-trapping was subsequently questioned by Grima^{16,17} in a model with a positive evaporation rate $\mu > 0$. Here it turned out that self-trapping is a transient phenomenon at $\mu > 0$ and crosses over to normal diffusion at very long times even for $d = 1, 2$. For sufficiently strong negative chemotaxis, Grima found long-time diffusive or *ballistic* motion depending on the secretion rate λ_e . This result which was obtained for any dimensionality d suggests that a particle might *self-propel* if it avoids the region where it has been in the past, and in some sense constitutes a link between repulsive autochemotaxis and the rapidly growing research field of active particle or microswimmers.^{7,9,18} (Note however, that while self-propulsion due to autochemorepulsion might apply to particles on a surface, for microorganisms

in bulk, which oblige momentum conservation, self-propulsion based on autochemorepulsion is conceptually not immediate and would probably need to involve some combination of parity-symmetry breaking and phoresis.)

Now we shall mainly review subsequent studies which include Brownian noise due to solvent molecules acting on the self-driven particles. Noise statistics is a relevant part of the actual trajectories of self-propelled particles⁸ both for microorganisms and synthetic microswimmers.^{19–21} It is expected that noise will destroy the perfect localization for positive autochemotaxis as well as the ballistic long-time motion for negative autochemotaxis. Indeed this was confirmed by numerical work and theoretical analysis in a subsequent paper of Sengupta et al²² which we shall discuss in the following in more detail.

The governing equations of the Brownian noise model introduced by Sengupta et al²² describe a coupling between the diffusion equation of the chemical concentration field $c(\vec{r}, t)$ and the trajectory of the secreting particle $\vec{r}_p(t)$. At vanishing evaporation rate μ , the chemical is emitted with a constant rate λ_e and is diffusing in d spatial dimensions according to

$$\frac{\partial c(\vec{r}, t)}{\partial t} = D_c \nabla^2 c(\vec{r}, t) + \lambda_e \delta(\vec{r} - \vec{r}_p(t)) \quad (21)$$

The equation of motion for the emitting particle is given by

$$\gamma \dot{\vec{r}}_p(t) = \vec{F}(\vec{r}_p, t) + \vec{\eta}(t) \quad (22)$$

Here, $\vec{\eta}(t)$ is an effective Gaussian white noise which zero mean and variance

$$\langle \eta_i(t) \eta_j(t') \rangle = 2\gamma\beta^{-1} \delta_{ij}(t - t') \quad (23)$$

with i and j denoting the Cartesian spatial components and β an effective inverse thermal energy. In Ref.²² the chemotactic force $\vec{F}(\vec{r}_p, t)$ depends on the history of the particle trajectory $\vec{r}_p(t)$ apart from a delay (or memory) time t_0 which takes into account that a finite time is needed for sensing the chemical. Integrating or superimposing over the Green's function of chemical diffusion, Eq.(2), the chemotactic force $\vec{F}(\vec{r}_p, t)$, Eq. (18), is modelled as

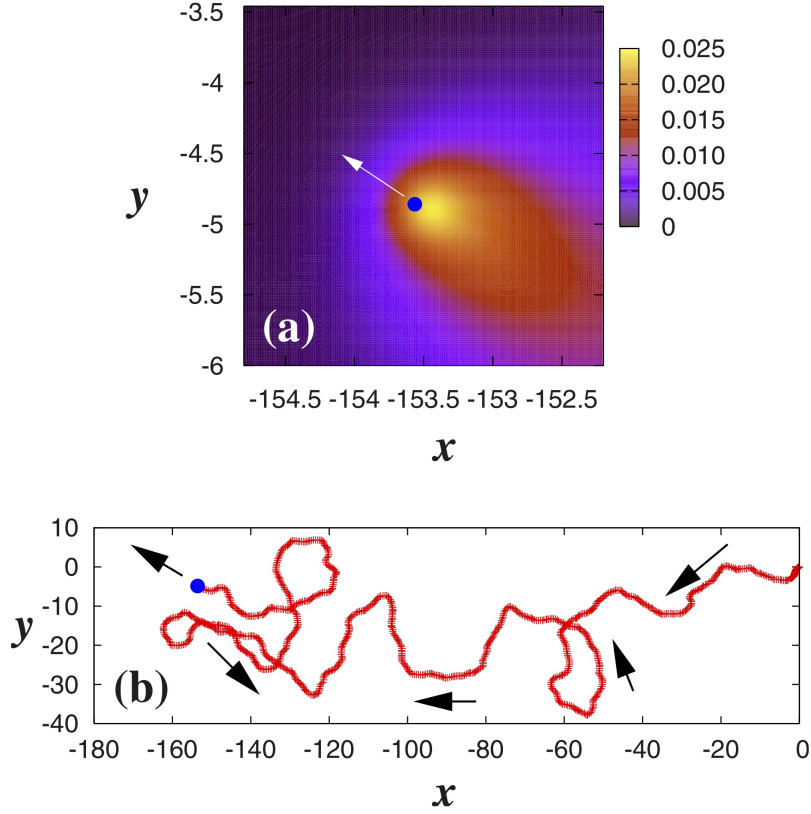


Fig. 2. (a) Snapshot of the instantaneous density profile $c(x, y)$ of the chemorepellent released by the microorganism moving in two dimensions, obtained from simulation, at time instant $t = 10.0$ (in units of λ_e^{-1}). (b) The entire trajectory, shown as the red (thick) curve, of the microorganism. The current position of the microorganism \vec{r}_p is indicated by the blue (black) dot in both the figures, and the direction of motion is indicated by arrows along the trajectory. The corresponding coupling strength being $|\lambda| = 10000$. The parameters are $D \equiv 1/\beta\gamma = 0.1\ell_o^2/\tau_o$, $D_c/D = 100$, $t_0 = 0.001\tau_o$ with length, time and energy scales of $\ell_0 = \sqrt{\sqrt{D_c D}/\lambda_e}$, $\tau_0 = 1/\lambda_e$, $1/\beta$. Figure from Ref.²²

$$\vec{F}(\vec{r}, t) = -2\alpha\lambda_e \int_0^{t-t_0} dt' \frac{(\vec{r} - \vec{r}_p(t')) \exp\left[\frac{-(\vec{r} - \vec{r}_p(t'))^2}{4D_c|t-t'|}\right]}{4D_c|t-t'| (4\pi D_c|t-t'|)^{d/2}} \quad (24)$$

For $d = 2$, a typical particle trajectory in the chemorepellent case and the associated chemical density field are shown in Figure 2. Clearly the

particle avoids its own trail where it had been in the past giving rise to a persistent random walk along the arrow shown in 2.

Results for the "exact" numerical solution of these governing equations are presented in Figure 3 for the chemoattractive case. There is long-time diffusive behaviour with a long-time diffusion coefficient D_l but for stronger couplings α , an intermediate transient time region shows up where the particle is quasi-localized. This localization is most pronounced in low spatial dimensions d . The long-time self-diffusion coefficient D_l drops strongly with the coupling α for any d (see Figure 3(d)) and scales with $1/\alpha^2$ in agreement with scaling arguments proposed in Ref.²²

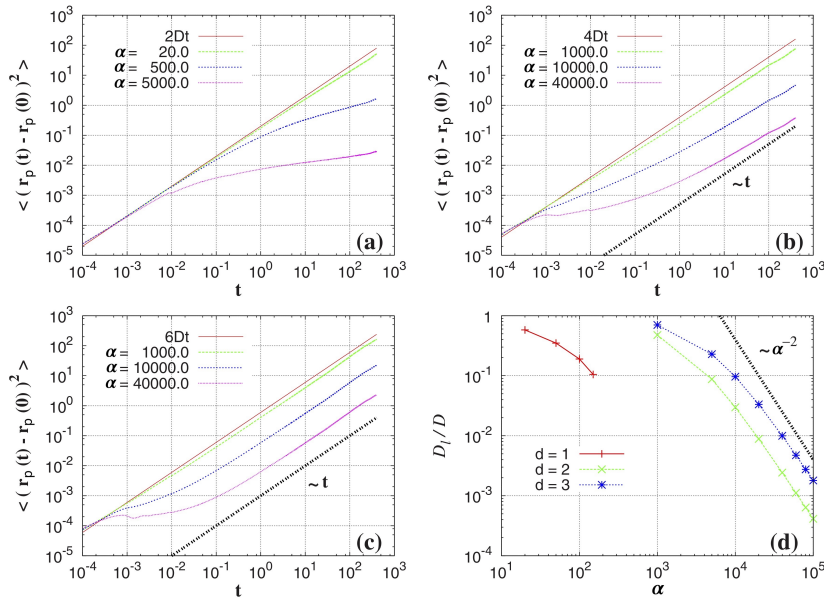


Fig. 3. Mean-square displacement $\langle [\vec{r}_b(t) - \vec{r}_b(0)]^2 \rangle$ of the microorganism as a function of time t with chemoattractant in (a) $d = 1$ with $\alpha = 20, 500, 5000$; (b) $d = 2$ with $\alpha = 1000, 10000, 40000$; (c) $d = 3$ with $\alpha = 1000, 10000, 40000$. The nonchemotactic diffusion reference lines are also indicated as $2Dt, 4Dt$, and $6Dt$ correspondingly for $d = 1, 2, 3$. Reference lines (thick dotted) are used to indicate the long-time diffusive behavior ($\sim t$) wherever possible. The relative long-time diffusivity D_l/D is shown as a function of α in (d) for $d = 1, 2, 3$. The reference line (thick dotted) shows a power-law scaling behavior $1/\alpha^2$ (see text). The parameters are as in 2, $D = 1/\beta\gamma$ is the short-time particle diffusivity and the coupling parameter α is measured in terms of ℓ_0^d/β . Figure from Ref.²²

Figure 4 shows the chemorepulsive case. Here, we again have a transient ballistic regime which is most pronounced in low spatial dimensions. A simple theory put forward in Ref.²² describes the strong increase of the long-time particle diffusivity with the coupling strength $|\lambda|$.

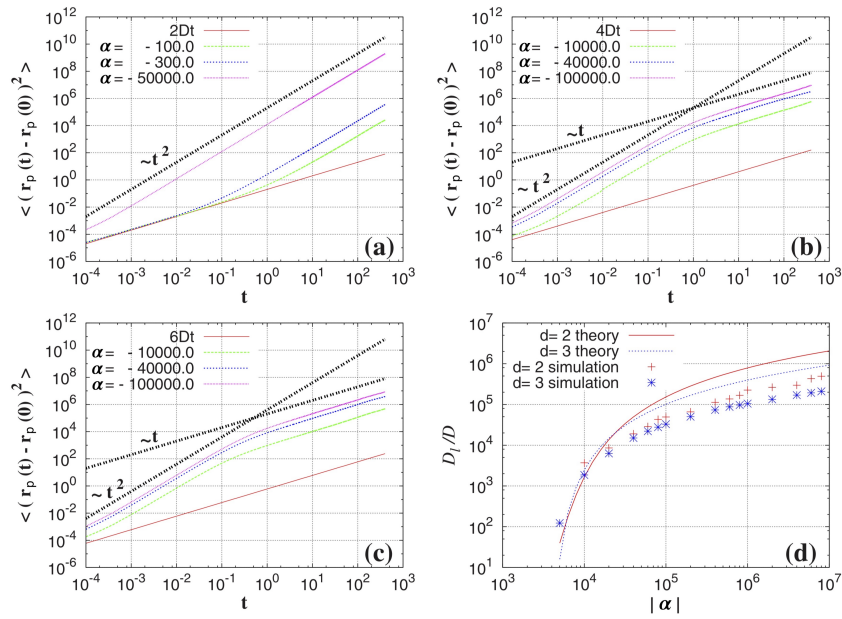


Fig. 4. Mean-square displacement $\langle [\vec{r}_b(t) - \vec{r}_b(0)]^2 \rangle$ of the microorganism as a function of time t with chemorepellent in (a) $d = 1$ with $\alpha = -100, -300, -50000$; (b) $d = 2$ with $\alpha = -1000, -40000, -100000$; (c) $d = 3$ with $\alpha = -1000, -40000, -100000$. The nonchemotactic diffusion reference lines are also indicated as $2Dt, 4Dt$, and $6Dt$ correspondingly for $d = 1, 2, 3$. Reference lines (thick dotted) indicating the ballistic ($\sim t^2$) and the long-time diffusive ($\sim t$) dynamics is shown as guide to the eye. The relative long-time diffusivity D_l/D is shown as a function of $|\alpha|$ in (d) for $d = 2, 3$. The points represent the actual data obtained from simulations, the lines correspond to a semiquantitative theory (see text). The parameters are as in Figure 2, $D = 1/\beta\gamma$ is the short-time particle diffusivity and the coupling parameter α is measured in terms of ℓ_0^d/β . Figure from Ref.²²

At this stage we mention that it is now possible to create synthetic particles which react in principle such that they avoid their own secretion trail. One important example discussed recently is an oil droplet in an aqueous surfactant solution which “remembers” the surfactant concentration which constitutes its self-propagation.²³ Another idea is to dynamically control

the motion of colloidal particles by optical fields which are dynamically adapted (programmed) such that the colloids avoid positions where they have been at earlier times; this leads to self-propulsion.²⁴ A third realization in the macroscopic world are robots which can be programmed at wish.²⁵ Moreover there are further but related theoretical models for particles avoiding their own past trails^{26,27} or involve memory effects leading to similar phenomena.^{28,29}

4. Chemotactic predator-prey dynamics

Next we shall explore two particles which are sensing each other via chemotaxis mimicking signaling among microorganisms. One particle ("predator") is attracted by the chemical secreted by the second particle and the latter ("prey") is repelled by the chemical secreted by the first one. Here we follow the model of Ref.¹⁰ Now we have two chemicals characterized by concentration fields $c_i(\vec{r}, t)$ ($i = 1, 2$) and two trajectories $\vec{r}_i(t)$. In the absence of chemical evaporation ($\mu = 0$), the concentration fields read

$$c_i(\vec{r}, t) = \lambda_i \int_0^t dt' \frac{1}{(4\pi D_{ci}|t-t'|)^{\frac{d}{2}}} \exp\left(-\frac{[\vec{r}-\vec{r}_i(t')]^2}{4D_{ci}|t-t'|}\right) \quad (25)$$

which is the solution of the chemical diffusion equation for given trajectories $\vec{r}_i(t)$ with D_{ci} denoting the diffusion coefficient of the two chemicals and λ_i being the production rate of chemical species i . The equations of motion determining the predator trajectory reads:

$$\gamma_1 \dot{\vec{r}}_1 = +\alpha_1 \nabla c_2(\vec{r}_1, t) + \vec{\eta}_1(t) \quad (26)$$

and the equation of motion for the prey is

$$\gamma_2 \dot{\vec{r}}_2 = -\alpha_2 \nabla c_1(\vec{r}_2, t) + \vec{\eta}_2(t) \quad (27)$$

where $\gamma_{1,2}$ are friction coefficients and $\alpha_{1,2}$ are chemotactic coupling coefficients.

As in Eq. (22) we generally allow for Gaussian white noise, represented by $\vec{\eta}_{1,2}(t)$.

It is important to remark here that the chemically mediated interaction between the predator and the prey is nonreciprocal, i.e. the force exerted by the predator acting on the prey is unequal to the force acting on the predator due to the prey particle. This violation of Newton's

third law stems from the non-equilibrium conditions and applies to the *effective interaction* among predator and prey; the microscopic interactions among all solvent molecules, and the predator and the prey particle are of course reciprocal so that momentum conservation applies and any net motion of the predator-prey-pair (in bulk) will be generally balanced by a counter-propagating flow of solvent (and or chemicals). Such nonreciprocal interactions are frequently encountered in situations away from equilibrium, e.g. in dusty plasmas.³⁰

A typical snapshot in the noise-free case is shown in Figure 5 which highlights the two concentration fields and the predator (left particle) following the prey (right particle).

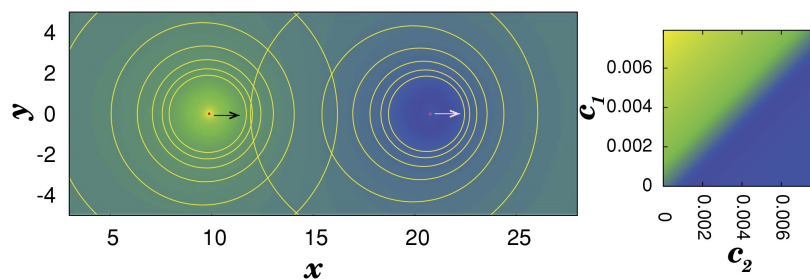


Fig. 5. (Left) A predator (red dot on left) chases a prey (red not visible dot on right), while the latter tries to escape through chemotactic gradient sensing of the diffusing chemicals. The arrows indicate their respective direction of motion in the absence of fluctuations. The contours around each microbe represent the equiconcentration lines of the secreted chemicals in a two-dimensional projected plane in this case, indicating the asymmetry of the distribution. The color code used here for the spatial distribution of the secreted chemorepellant (c_1) and the chemoattractant (c_2), as they mingle in space, is shown in the right panel. Figure from Ref.¹⁰

As a result of the analysis performed in Ref.,¹⁰ there are basically two dimensionless parameters which govern the escape and chase scenario, still in the case of vanishing noise. The first parameter is the reduced length scale Δ^* depending on r_{12} which is the steady-state distance between the particles; the second parameter is a sensibility ratio δ ; see¹⁰ for details. The state diagram is shown in Figure 6 in the parameter plane, spanned by Δ^* and δ , and shows regions of escape and capture. For $\delta > 1$ there is always trapping, independent of the initial conditions. For $\delta < 1$ it depends on the initial particle separation r_0^* (see Figure 6b) which effective Δ^* is realized.

On the separation line there is steady state motion with a constant particle separation, i.e. both particles move with the same speed. This line can be calculated analytically and is given by

$$\delta(\Delta^*) = (1 + \Delta^{*-1}) \exp(-\Delta^{*-1}) \quad (28)$$

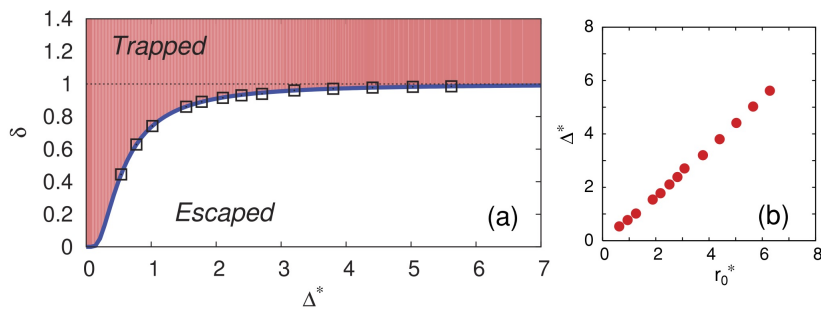


Fig. 6. (a) Dynamical phase diagram of the chemotactic predator-prey system, constructed in the $\Delta^* - \delta$ parameter space, showing the trapped (shaded) and escaped phases. The phase boundary (thick solid line) is obtained analytically and matches the simulation data (boxes). The horizontal thin dotted line ($\delta = 1$) represents the upper bound for the trapped-to-escaped dynamical phase transition (see text). (b) The dependence of the catching range (Δ^*) on the initial separation (r_0^*), as obtained from simulations. Figure from Ref.¹⁰

The particular form of the diffusing chemical field in the absence of evaporation, Eq. (17), allows the prediction of two scaling laws. The first one applies to escape situations and shows that the distance x between the two particles increases subdiffusively with time t as $t^{1/3}$, while the second one applies to trapping situations and predicts that the distance between predator and prey decreases as $(t_{trap} - t)^{1/3}$ with a finite trapping time t_{trap} where $x = 0$.

As a final remark, there are also other predator-prey models which model the predator and prey dynamics either on a lattice³¹ or with more complex models designed for real bacteria.³² A marvellous realization of a synthetic predator-prey system employs a pair of an ion-exchange resin and a passive charged colloidal particle which moves autonomously as a "modular swimmer";³³ another interesting realization of a predator-prey-like pair is based on two different particles, which are actuated as a pair.³⁴

5. Collective behavior of few and many active particles

Tsori and de Gennes¹⁵ have pointed out the analogy between chemoattractive matter and *gravity* in three spatial dimensions. In fact, the chemotactic coupling (18) together with the Coulomb orbitals (9) and the linearity of the diffusion equations implies that a one-component system is identical to gravitating particles. The dynamics will lead to clustering and finally to a collapse ("black hole"). Hence one can study aspects of the dynamics of a black hole collapse scaled down in a Petri dish, see e.g. Ref.³⁵ for a similar idea.

Binary mixtures of particles with chemotactic coupling coefficients of opposite sign lead to a similar physical behavior as oppositely electrically charged mixtures. These systems form interesting cluster structures and lead to effectively non-reciprocal forces, i.e. they break Newton's third law *actio=reactio*. These nonreciprocal forces can lead to self-propulsion and self-rotation³⁶ which only emerges if different colloids closely approach each other and form "active molecules" appearing in a broad variety of shapes as movers, rotators and circle swimmers.^{34,37,38} The simplest example of such an active molecule is a moving dimer similar to the predator-prey system discussed in the previous chapter. A direct experimental confirmation of active molecules consisting of two species was found in Ref.³⁹ where two different types of ion exchange resins provide the active constituents.

The full many-body behavior of a binary mixture interacting with chemotactic-based nonreciprocal interactions was studied in Refs.,⁴⁰ however in the different context of complex plasmas. In Ref.,³⁶ the connection to chemotaxis was worked out explicitly. One example for the collective behaviour in a binary system of chemotactically coupled species is shown in Figure 7 at vanishing noise. On the x -axis a relative wake charge is plotted which corresponds to the non-reciprocity governed by the asymmetry in the sensing mechanisms of the two particles. The y -axis shows the two-dimensional particle density. There is a rich steady state diagram with four different dynamical states involving inactive (i.e. non-moving) states and active ones. The latter are either swarms or orientationally disordered active fluids.

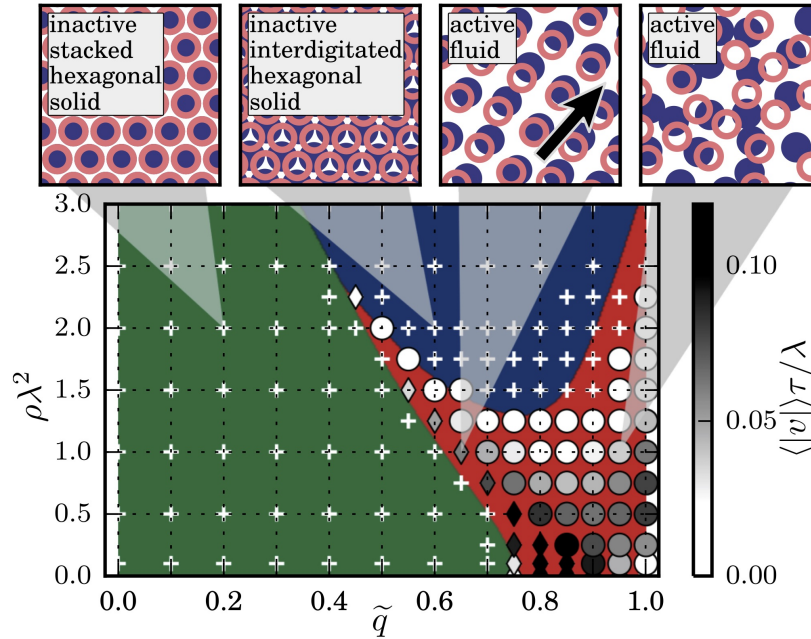


Fig. 7. State diagram in the zero-temperature limit, plotted in the plane of a reduced number density ρ and relative wake charge \tilde{q} . Color coding depicts results obtained from the stability analysis, symbols show numerical results. Inactive systems (+) can be either *stacked hexagonal solid* (green background) or *interdigitated hexagonal solid* (blue background). For *active fluid* regimes (o, red background), the average particle velocities are indicated by a gray scale. Diamonds (\diamond) are used instead of circles if active doublets emerge whose decay time τ_D exceeds a threshold of $10^3\tau$. The states are illustrated by typical snapshots. Figure from Ref.⁴⁰

A further interesting setup of particles interacting via chemotaxis is provided by autophoretic Janus colloids. These particles catalyze a chemical reaction on part of their surface only resulting in a chemical gradient across their own surface. This self-produced gradient sets them into motion via diffusiophoresis or a similar mechanism. Remarkably, a Janus colloid does not only respond to self-produced gradients, but also to gradients produced by other Janus colloids, essentially by chemotaxis (or taxis with respect to another phoretic field). Thus, phoretic Janus colloids interact “chemically” and provide a synthetic analogon to microbiological signaling.^{14,41,42} These chemical interactions play a crucial role for the collective behaviour

of large suspensions of Janus colloids⁴³ and can generate patterns including clusters,^{41–45} traveling waves⁴³ and continuously moving patterns⁴² and in case of chiral active particles also spiral patterns and phase separation with traveling waves emerging within the dense phase.⁴⁶

6. Conclusions

In conclusion, we have discussed models for chemotactic behavior of microorganisms and synthetic particles in a diffusing chemical concentration field focusing on three different scenarios: i) autochemotaxis of a single particles, ii) predator-prey models arising from chemotactic coupling to two different chemicals secreted by the predator and the prey, iii) clusters and collective behavior of many particles coupled via their chemotactic response to chemical fields produced by other particles. Here, attractive autochemotaxis may lead to self-localization while repulsive autochemotaxis leads to trajectories avoiding their own past. We have also discussed that a moving chemotactic source leads to a front-rear asymmetry in the chemical field resulting in marked scaling laws for predator-prey systems. Finally, chemotaxis in multi-species systems provides an avenue towards a new world of active molecules where we have just started to tap the full potential of the novel cluster formation processes. Collective behavior includes a swarming of chemotactically coupled particles at finite concentrations.

We close with an outlook to future problems. First, at high chemical concentration or strongly coupled chemical fields, the simple diffusion equation picture will break down, calling for new models. This is in particular important for multivalent microions at high concentrations. Recent developments have considered these effects of strong coupling in using nonlinear diffusion equations. These equations can be based on the dynamical version of classical density functional theory, so-called dynamical density functional theory (DDFT).^{47–50} In this framework, the equations of motion of a chemical around a point source are given by

$$\frac{\partial c(\vec{r}, t)}{\partial t} = D \vec{\nabla}_c(\vec{r}, t) \vec{\nabla} \frac{\delta \mathcal{F}[c(\vec{r}, t)]}{\delta c(\vec{r}, t)} - \mu c(\vec{r}, t) + \lambda_e \delta(\vec{r}) \quad (29)$$

where $\mathcal{F}[n(\vec{r})]$ is the equilibrium free energy density functional.^{51–53} For a noninteracting system (ideal gas), the functional is known explicitly and in this limit the traditional diffusion equation (1) is recovered. Nontrivial particle correlations as arising from interactions among the chemical species are contained in the functional in the general case and

make the diffusion equation nonlinear. In certain cases, linearization is possible and corresponding analytical solutions for the Green's function of diffusing interacting particles can indeed be found within DDFT.⁵⁴

A second important generalization concern time-dependent secreting rates as embodied in a non-constant function $\lambda_e(t)$ such as e.g. an emission rate that is periodic in time. This situation has recently been considered⁵⁴ and leads to propagating density waves of the chemical around the emitting source. Again, in some special cases, the Green's function can be found analytically within DDFT.⁵⁴

Third, in terms of predator-prey models, the situation of a single predator and a single prey can be generalized towards a herd of prey and to a group of chasers. This has been discussed in the literature within different models, see e.g.⁵⁵⁻⁵⁸ but needs to be extended within the chemotactic context. Efficient chase and escape strategies⁵⁹ may depend on the details of predator/prey perception.

Fourth, most of our consideration were done in the bulk. Confinement near system walls and crowding situations will change both the diffusion of the chemical as well as the chemotactic dynamics. Similarly, chemotaxis in complex environments, such as traveling waves may lead to interesting transport effects.⁶⁰ We are just at the beginning of a systematic understanding of chemotaxis in complex environment.

Finally we have considered the evaporation of different chemicals by a constant rate in our modelling. If two different chemicals which e.g. govern a predator-prey system or the formation of the active molecule, react between themselves this would constitute a more complicated and highly interesting problem with new scenarios induced by coupling nonlinear reaction-diffusion equations to the chemical kinetics and the particle motions.

7. Acknowledgements

H.L. gratefully acknowledges support by the Deutsche Forschungsgemeinschaft (DFG) through grant LO 418/19-1.

References

1. M. Kollmann, L. Lovdok, and K. Bartholome, Design principles of a bacterial signalling network, *Nature*. **438**, 504 (2005).

2. U. B. Kaupp, N. D. Kashikar, and I. Weyand, Mechanisms of sperm chemotaxis, *Annu. Rev. Physiol.* **70**, 93 (2008).
3. W. C. K. Poon, Soft matter: From synthetic to biological materials, *Lecture Notes of the 39th IFF Spring School, Forschungszentrum Julich GmbH.* **11**, 1 (2008).
4. C. Hoell and H. Löwen, Theory of microbe motion in a poisoned environment, *Phys. Rev. E.* **84**, 42903 (2011).
5. R. Metzler and J. Klafter, The random walk's guide to anomalous diffusion: a fractional dynamics approach, *Phys. Rep.* **339**, 1 (2000).
6. E. J., R. G. Winkler, and G. Gompper, Physics of microswimmers—single particle motion and collective behavior: a review, *Rep. Prog. Phys.* **78**, 56601 (2015).
7. A. Zoettl and H. Stark, Emergent behavior in active colloids, *J. Phys. Condens. Matter.* **28**, 253001 (2016).
8. C. Bechinger, R. Di Leonardo, H. Löwen, C. Reichhardt, G. Volpe, and G. Volpe, Active particles in complex and crowded environments, *Rev. Mod. Phys.* **88**, 045006 (2016).
9. A. M. Menzel, Tuned, driven, and active soft matter, *Phys. Rep.* **554**, 1 (2015).
10. A. Sengupta, T. Kruppa, and H. Löwen, Chemotactic predator-prey dynamics, *Phys. Rev. E.* **83**, 31914 (2011).
11. J.-P. Hansen and H. Löwen, Effective interactions between electric double-layers, *Annu. Rev. Phys. Chem.* **51**, 209 (2000).
12. H. Löwen, Charged rodlike colloidal suspensions: An ab initio approach, *J. Chem. Phys.* **100**, 6738 (1994).
13. J. D. Murray, *Mathematical biology. II spatial models and biomedical applications {Interdisciplinary Applied Mathematics}*. Springer-Verlag Berlin Heidelberg (2003).
14. M. Meyer, L. Schimansky-Geier, and P. Romanczuk, Active brownian agents with concentration-dependent chemotactic sensitivity, *Phys. Rev. E.* **89**, 022711 (2014).
15. Y. Tsori and P.-G. de Gennes, Self-trapping of a single bacterium in its own chemoattractant, *EPL.* **66**, 599 (2004).
16. R. Grima, Strong-coupling dynamics of a multicellular chemotactic system, *Phys. Rev. Lett.* **95**, 128103 (2005).
17. R. Grima, Phase transitions and superuniversality in the dynamics of a self-driven particle, *Phys. Rev. E.* **74**, 011125 (2006).
18. G. Gompper, C. Bechinger, S. Herminghaus, R. E. Isele-Holder, U. B. Kaupp, H. Löwen, H. Stark, and R. G. Winkler, Microswimmers - from single particle motion to collective behaviour, *Eur. Phys. J. ST.* **226**, 2061 (2016).
19. B. ten Hagen, S. van Teeffelen, and H. Löwen, Brownian motion of a self-propelled particle, *J. Phys. Condens. Matter.* **23**, 194119 (2011).
20. X. Zheng, B. ten Hagen, A. Kaiser, M. Wu, H. Cui, Z. Silber-Li, and H. Löwen, Non-gaussian statistics for the motion of self-propelled janus particles: Experiment versus theory, *Phys. Rev. E.* **88**, 032304 (2013).
21. F. Kümmel, B. ten Hagen, R. Wittkowski, I. Buttinoni, R. Eichhorn,

- G. Volpe, H. Löwen, and C. Bechinger, Circular motion of asymmetric self-propelling particles, *Phys. Rev. Lett.* **110**, 198302 (2013).
22. A. Sengupta, S. van Teeffelen, and H. Löwen, Dynamics of a microorganism moving by chemotaxis in its own secretion, *Phys. Rev. E.* **80**, 31122 (2009).
 23. C. Jin, C. Krüger, and C. C. Maass, Chemotaxis and autochemotaxis of self-propelling droplet swimmers, *Proc. Natl. Acad. Sci.* **114**, 5089 (2017).
 24. J. Bewerunge, A. Sengupta, R. F. Capellmann, F. Platten, S. Sengupta, and S. U. Egelhaaf, Colloids exposed to random potential energy landscapes: From particle number density to particle-potential and particle-particle interactions, *J. Chem. Phys.* **145**, 044905 (2016).
 25. M. Mijalkov, A. McDaniel, J. Wehr, and G. Volpe, Engineering sensorial delay to control phototaxis and emergent collective behaviors, *Phys. Rev. X.* **6**, 011008 (2016).
 26. W. T. Kranz, A. Gelimson, K. Zhao, G. C. L. Wong, and R. Golestanian, Effective dynamics of microorganisms that interact with their own trail, *Phys. Rev. Lett.* **117**, 038101 (2016).
 27. A. Gelimson and R. Golestanian, Collective dynamics of dividing chemotactic cells, *Phys. Rev. Lett.* **114**, 028101 (2015).
 28. J. Taktikos, V. Zaburdaev, and H. Stark, Modeling a self-propelled autochemotactic walker, *Phys. Rev. E.* **84**, 041924 (2011).
 29. C. Valeriani, R. J. Allen, and D. Marenduzzo, Non-equilibrium dynamics of an active colloidal "chucker", *J. Chem. Phys.* **132**, 204904 (2010).
 30. A. V. Ivlev, J. Bartnick, M. Heinen, C.-R. Du, V. Nosenko, and H. Löwen, Statistical mechanics where Newton's third law is broken, *Phys. Rev. X.* **5**, 011035 (2015).
 31. G. Oshanin, O. Vasilyev, P. L. Krapivsky, and J. Klafter, Survival of an evasive prey, *Proc. Natl. Acad. Sci.* **106**, 13696 (2009).
 32. H. Jashnsaz, G. G. Anderson, and S. Presse, Statistical signatures of a targeted search by bacteria, *Phys. Biol.* **14**, 065002 (2017).
 33. R. Niu, D. Botin, J. Weber, A. Reinmüller, and T. Palberg, Assembly and speed in ion-exchange-based modular phoretic microswimmers, *Langmuir.* **33**, 3450–3457 (2017).
 34. F. Schmidt, B. Liebchen, H. Löwen, and G. Volpe, Light-controlled assembly of active colloidal molecules, *arXiv:1801.06868 (J. Chem. Phys., in press)* (2018).
 35. J. Bleibel, S. Dietrich, A. Domínguez, and M. Oettel, Shock waves in capillary collapse of colloids: A model system for two-dimensional screened Newtonian gravity, *Phys. Rev. Lett.* **107**, 128302 (2011).
 36. J. Bartnick, M. Heinen, A. V. Ivlev, and H. Löwen, Structural correlations in diffusiophoretic colloidal mixtures with nonreciprocal interactions, *J. Phys. Condens. Matter.* **28**, 025102 (2016).
 37. R. Soto and R. Golestanian, Self-assembly of catalytically active colloidal molecules: Tailoring activity through surface chemistry, *Phys. Rev. Lett.* **112**, 068301 (2014).
 38. R. Soto and R. Golestanian, Self-assembly of active colloidal molecules with dynamic function, *Phys. Rev. E.* **91**, 052304 (2015).

39. R. Niu, T. Palberg, and T. Speck, Self-assembly of colloidal molecules due to self-generated flow, *Phys. Rev. Lett.* **119**, 028001 (2017).
40. J. Bartnick, A. Kaiser, H. Löwen, and A. V. Ivlev, Emerging activity in bilayered dispersions with wake-mediated interactions, *J. Chem. Phys.* **144**, 224901 (2016).
41. S. Saha, R. Golestanian, and S. Ramaswamy, Clusters, asters, and collective oscillations in chemotactic colloids, *Phys. Rev. E* **89**, 062316 (2014).
42. B. Liebchen, D. Marenduzzo, I. Pagonabarraga, and M. E. Cates, Clustering and pattern formation in chemorepulsive active colloids, *Phys. Rev. Lett.* **115**, 258301 (2015).
43. B. Liebchen, D. Marenduzzo, and M. E. Cates, Phoretic interactions generically induce dynamic clusters and wave patterns in active colloids, *Phys. Rev. Lett.* **118**, 268001 (2017).
44. O. Pohl and H. Stark, Dynamic clustering and chemotactic collapse of self-phoretic active particles, *Phys. Rev. Lett.* **112**, 238303 (2014).
45. O. Pohl and H. Stark, Self-phoretic active particles interacting by diffusio-phoresis: A numerical study of the collapsed state and dynamic clustering, *Euro. Phys. J. E* **38**, 93 (2015).
46. B. Liebchen, M. E. Cates, and D. Marenduzzo, Pattern formation in chemically interacting active rotors with self-propulsion, *Soft Matter* **12**, 7259 (2016).
47. U. M. B. Marconi and P. Tarazona, Dynamic density functional theory of fluids, *J. Chem. Phys.* **110**, 8032 (1999).
48. A. J. Archer and R. Evans, Dynamical density functional theory and its application to spinodal decomposition, *J. Chem. Phys.* **121**, 4246 (2004).
49. P. Espanol and H. Löwen, Derivation of dynamical density functional theory using the projection operator technique, *J. Chem. Phys.* **131**, 244101 (2009).
50. H. Löwen. Dynamical density functional theory for Brownian dynamics of colloidal particles. In ed. J. Wu, *Variational Methods in Molecular Modeling*, chapter 9, p. 255. Springer (2017).
51. R. Evans, The nature of the liquid-vapour interface and other topics in the statistical mechanics of non-uniform, classical fluids, *Adv. Phys.* **28**, 143 (1979).
52. Y. Singh, Density-functional theory of freezing and properties of the ordered phase, *Phys. Rep.* **207**, 351 (1991).
53. H. Löwen, Melting, freezing and colloidal suspensions, *Phys. Rep.* **237**, 249 (1994).
54. H. Löwen and M. Heinen, Dynamical density functional theory for the diffusion of injected brownian particles, *Eur. Phys. J. ST* **223**, 3113 (2014).
55. M. Schwarzl, A. Godec, G. Oshanin, and R. Metzler, A single predator charging a herd of prey: effects of self volume and predator-prey decision-making, *J. Phys. A* **49**, 225601 (2016).
56. C. Mejía-Monasterio, G. Oshanin, and G. Schehr, First passages for a search by a swarm of independent random searchers, *J. Stat. Mech.* **2011**, P06022 (2011).
57. R. Nishi, A. Kamimura, K. Nishinari, and T. Ohira, Group chase and escape

- with conversion from targets to chasers, *Physica A.* **391**, 337 (2012).
58. T. Saito, T. Nakamura, and T. Ohira, Group chase and escape model with chasers interaction, *Physica A.* **447**, 172 (2016).
 59. O. Bénichou, C. Loverdo, M. Moreau, and R. Voituriez, Intermittent search strategies, *Rev. Mod. Phys.* **83**, 81 (2011).
 60. A. Geiseler, P. Hänggi, F. Marchesoni, C. Mulhern, and S. Savel'ev, Chemotaxis of artificial microswimmers in active density waves, *Phys. Rev. E.* **94**, 012613 (2016).